

Numerical Simulation of the Daikai Station Subway Structure Collapse due to Sudden Uplift during Earthquake

著者	Kishi Norimitsu, Sonoda Keiichiro, Komuro Masato, Kawarai Tomoki
journal or publication title	JOURNAL OF ENGINEERING MECHANICS
volume	147
number	3
page range	04020152
year	2021
URL	http://hdl.handle.net/10258/00010452

doi: info:doi/10.1061/(ASCE)EM.1943-7889.0001895



Numerical Simulation of the Daikai Station Subway Structure Collapse due to Sudden Uplift during Earthquake

Norimitsu Kishi, Ph.D., M.ASCE¹; Keiichiro Sonoda, Ph.D.²; Masato Komuro, Ph.D.³; and Tomoki Kawai⁴

Abstract: The Daikai Station subway structure in Japan completely collapsed during the Hyogoken-Nanbu earthquake that occurred on January 17, 1995. Based on the numerical results obtained by two-dimensional finite-element analysis, the structure is believed to have collapsed as a result of strong lateral vibration. However, because it deformed in an approximately symmetrical manner with respect to the shortened central columns, it might have experienced catastrophic collapse due to vertical impulse motion. To investigate the dynamic response behavior of the structure due to sudden upward loading, a three-dimensional elastoplastic transient response analysis was conducted considering an isolated upward pulselike displacement wave from the bedrock. The results of this study suggest that the central column of the structure reached axial compression failure due to the amplitude of the displacement wave increasing significantly at the lower end of the column. This method can numerically reproduce the collapsed state of the structure and the considerable settlement of the ground surface due to the occurrence of the high-intensity earthquake. DOI: [10.1061/\(ASCE\)EM.1943-7889.0001895](https://doi.org/10.1061/(ASCE)EM.1943-7889.0001895). This work is made available under the terms of the Creative Commons Attribution 4.0 International license, <https://creativecommons.org/licenses/by/4.0/>.

Author keywords: Hyogoken-Nanbu earthquake; Daikai subway station; Impulse uplift; Elastoplastic response analysis; Transient response; Collapse of RC columns.

Introduction

Due to the Hyogoken-Nanbu (Hanshin-Awaji) earthquake that occurred on January 17, 1995, in southwestern Japan, many people's lives were lost, and many bridges and infrastructure components in the Kobe-Osaka area suffered severe damage. The registered magnitude of the earthquake was 7.2 on the Richter scale, and the focal depth was 16 km below ground level. The Kobe Ocean Meteorological Observatory Station located approximately 20 km northeast of the epicenter recorded peak ground accelerations of 8.2, 6.2, and 3.3 m/s² for the north-south (N-S), east-west (E-W), and up-down (U-D) components, respectively, and a peak ground velocity of 1.05 m/s.

Upon inspecting damage to the RC bridge piers, it was observed that many piers suffered severe damage by bending failure initiated near the end of the longitudinal rebar at the midheight section and by shear failure due to the small rebar volume for shear reinforcement under the strong lateral vibrations of the earthquake. Following this event, to avoid the aforementioned damage to RC piers due to destructive earthquakes such as the Hyogoken-Nanbu earthquake, the seismic design specifications for bridges were revised, and piers were strengthened nationwide in Japan based on these

specifications (Japan Road Association 1996; Kawashima and Unjoh 1997).

However, the compression failure of RC bridge piers, as shown in Fig. 1, and the collapse of the Daikai Station subway structure (Hanshin Expressway Public Corporation 1995) could have been caused by the observed vertical motion. In particular, the significant damage to the Daikai Station subway structure shown in Fig. 2 was the first severe failure case worldwide used to modify the general practice of structural and geotechnical engineers regarding underground structures with better seismic performance than surface structures because underground structures that do not cross an active fault are influenced by the deformation of the surrounding ground if there is no liquefaction during an earthquake and if they have a smaller unit weight than that of the subsoil. Because the structure was significantly deformed and approximately symmetrically with respect to the shortened central columns due to axial compression failure, it is not easy to explain how the damage was induced by the strong lateral vibration of the earthquake.

After the earthquake, many numerical simulations of the collapsed structure were performed based on two-dimensional (2D) finite-element (FE) analysis considering the nonlinear dynamic characteristics of the surrounding soils and using the registered ground motions near the station as inputs (EERC 1995; Iida et al. 1996; Matsuda et al. 1997; An et al. 1997; Maekawa et al. 2003; Huo et al. 2005; Parra-Monesinos et al. 2006). The results suggest that the distortion of the central column likely increased significantly due to strong lateral vibration; then, the columns completely collapsed due to the additional moment caused by the weight of the overburden soils.

Recently, Yu and Li (2017) and Li and Chen (2018) tried to simulate the collapse of the Daikai Station subway structure with a three-dimensional (3D) elastoplastic earthquake response analysis. The results indicated that the structure reached complete collapse, as shown by the numerical results obtained from 2D FE analysis. In particular, Yu and Li (2017) numerically investigated the effects of vertical ground motion on the collapse of the structure and suggested that the behavior of the central columns was mainly

¹Specially Appointed Professor, College of Engineering, Muroran Institute of Technology, Muroran, Hokkaido 050-8585, Japan (corresponding author). ORCID: <https://orcid.org/0000-0002-9685-5761>. Email: kishi@mmm.muroran-it.ac.jp

²Professor Emeritus, Dept. of Urban Engineering, Osaka City Univ., Sumiyoshi, Osaka 558-8585, Japan.

³Professor, College of Engineering, Muroran Institute of Technology, Muroran, Hokkaido 050-8585, Japan.

⁴Graduate Student, Div. of Engineering, Graduate School, Muroran Institute of Technology, Muroran, Hokkaido 050-8585, Japan.

Note. This manuscript was submitted on July 2, 2020; approved on October 19, 2020; published online on December 18, 2020. Discussion period open until May 18, 2021; separate discussions must be submitted for individual papers. This paper is part of the *Journal of Engineering Mechanics*, © ASCE, ISSN 0733-9399.



Fig. 1. (Color) Example of the compression failure of an RC bridge pier. (Image by Keiichiro Sonoda.)



Fig. 2. (Color) Compression failure of the central columns of the Daikai Station subway structure. (Reprinted with permission from Sakurai 2014.)

controlled by the lateral ground motion and that vertical motion could be neglected. However, the behavior of a central column that reaches axial compressive failure and is subjected to strong lateral vibration of the earthquake has not been directly and numerically

analyzed by using not only 2D FE analysis methods but also 3D FE analysis methods. It was depicted that the station structure deformed laterally instead of symmetrically, which is different from the actual damage state of the station structure. Huo et al. (2005) concluded that the columns yielded in flexure at a drift ratio of approximately 0.5%–0.7% and then drastically lost capacity with inadequate transverse reinforcement under a large axial load. Maekawa et al. (2003) predicted that the columns might collapse based on the application of a static failure interaction diagram in terms of compressive stress and normalized displacement.

According to verbal evidence from the inhabitants of the region regarding their experiences at the beginning of the earthquake (Sonoda et al. 1997a), many people experienced the following:

- ground uplift, e.g., “at first, it was pushed up with a bang and laterally vibrated” and/or “his body floated in the air”;
- jumping phenomena, for example “a heavy safe jumped up and broke through the ceiling” and/or “a 4-ton dump truck waiting for a traffic signal jumped up several times”; and
- seaquake phenomena, e.g., “a fishing boat was lifted up according to fisherman” and/or “according to the captain, a luxury passenger liner at sea near Kobe suffered severe impact several times greater than that of a water hammer.”

Regarding seaquakes, based on the analytical results of elastodynamic wave interaction analysis in a one-dimensional seabed-seawater system, Uenishi and Sakurai (2014) indicated that seaquakes may be induced by resonance between the system and the incident P wave component of an earthquake.

Regarding seismographs that are used to record the earthquake waves when the Hyogoken-Nanbu earthquake occurred, it was clarified that the Kobe Ocean Meteorological Observatory Station employed an acceleration type of seismograph and recorded the time histories of the waves with sampling intervals of 0.01 s. The waves were filtered through the low-pass cutoff frequencies of 10 Hz. Even though there were many pieces of verbal evidence from the inhabitants regarding sudden uplift, which was previously mentioned, there is no clear actual digital evidence whether the actual Hyogoken-Nanbu earthquake had frequency components higher than 10 Hz and a peak ground velocity faster than 1.5 m/s.

Knowing that high-frequency vertical components are not measured when using seismometers but may be present in actual earthquake waves, Sonoda and Kobayashi (1996) performed elastic stress-wave propagation analyses for an RC bridge pier model supported by a multilayered ground model subjected to a seismically induced modified isolated sinusoidal compressive half wave with a short period. The results were used to clarify whether the high-frequency characteristics of the vertical ground motion during an earthquake had a significant effect on the impactlike failure of the column due to large axial tensile and compressive stresses; additionally, they tried to numerically analyze the Daikai Station subway model for a single vertical displacement wave transmitted from the base stratum and indicated that the central columns in the structure might collapse due to an incident wave with an approximately 80-ms period (Sonoda et al. 1997b). Uenishi and Sakurai (2000) also analyzed elastic compressive wave propagation through columns supporting overburden soils subjected to vertical oscillation and indicated that the central columns in the Daikai Station subway structure could fail if the incident wave was approximately 17 Hz for the dominant frequency.

As described previously, the Daikai subway structure might collapse due to an earthquake due to strong lateral ground motion or vertical motion with comparatively high-frequency components. Currently, with the high-speed processing power of computers and the development of numerical calculation techniques, prototypes

can be developed, and increasingly complicated elastoplastic dynamic response analyses of concrete cracking and axial compression failure are no longer difficult to perform.

In this paper, to investigate the dynamic behavior of the Daikai subway structure and the potential for collapse of the central columns in the structure subjected to an isolated pulselike upward displacement wave from the bedrock instead of strong lateral vibration during the Hyogoken-Nanbu earthquake, a 3D elastoplastic transient response analysis was performed considering the surrounding soils, a varying input velocity, and the period of displacement loading. In this study, two kinds of load durations were considered: 5 and 50 ms, which are estimated as periods of 10 and 100 ms, respectively. The commercial nonlinear dynamic response analysis program LS-DYNA version R9.1.0 (Livermore Software Technology Corporation 2016) was used in this study.

Research Significance

To clarify the failure mechanism of the central columns of the Daikai Station subway structure during the Hyogoken-Nanbu earthquake, 2D and/or 3D FE earthquake response analyses were conducted by many researchers. Even though almost all researchers concluded that the distortion of the columns increased significantly due to the strong lateral vibration and then the columns completely failed due to the weight of the overburdened soil, the failure behaviors of the columns have not been analyzed numerically and the behavior was predicted only based on the static failure mechanisms.

The research presented in this paper is an attempt to numerically investigate the possibility of the collapse of the central column that was subjected to a sudden uplift with a comparatively short duration of less than 0.1 s by using a 3D elastoplastic transient response analysis method, which is based on the damage patterns of the Daikai Station subway structure during the Hyogoken-Nanbu earthquake. The sudden uplift wave could not be recorded at the Kobe Ocean Meteorological Observatory Station and might have occurred prior to the strong lateral vibration. Numerical analysis was performed from the beginning of the sudden uplift at the base stratum to the central column, which reaches axial compression failure, and the ground surface subsides due to gravity. The failure mechanism of the central column was investigated using time histories of the displacement and particle velocity at each point from the bedrock to the ground surface and the deformation and crack patterns of the structure after numerical calculation. The results point out that the central columns of the station structure may collapse with the mode of axial compression failure due to the sudden uplift, among others.

Daikai Subway Station

The subway structure of Daikai Station, which is part of the Kobe Rapid Railway System, was constructed underground along National Highway No. 28 via the cut-and-cover method between 1962 and 1964. The station is located approximately 15 km from the epicenter of the earthquake and consists of three parts: the main section of the station, the access station section with two underground levels, and a tunnel. Figs. 3(a and b) show the schematic damage patterns of the station structure (Sato Kogyo Co. Ltd. 1997). Fig. 3(a) shows the longitudinal damage patterns. As shown in this figure, during the earthquake, 23 central columns of the main section collapsed completely over a total length of approximately 80 m, and this process caused the failure of the ceiling slab and a maximum subsidence of 2.5 m for National Highway No. 28 above

the station [Fig. 3(b)]. However, the access station section and the tunnel connected to the station did not suffer severe damage. More detailed damage data of the station structure were reported by Iida et al. (1996).

As shown in Fig. 3(b), the main section of the station has a 4.8-m-thick overburden soil layer and consists of an RC box structure with a width of 17 m and height of 7.17 m; this section is supported by the central columns through the upper and lower girders, which are designed with a center-to-center spacing of 3.5 m in the longitudinal direction. The central column is 3.82 m high with a cross section of 0.4×1.0 m. Round steel bars of 16–25 mm in diameter were used as reinforcements for the walls and slabs. The central columns were axially reinforced with 30 rebar pieces with a 32-mm diameter and tied using rebar pieces with 9-mm diameters at 350-mm intervals.

The restoration of the station structure was officially authorized on February 28, 1995. Even though the original station structure was designed without considering any seismic effects, seismic design for the new structure was performed based on the response deformation method by using velocity response spectra, which were obtained using the earthquake record for the depth of 83 m at Kobe Port Island. Each wall and column were designed following the limit-state design methods, in which the vertical ground motions were taken into account as a vertical static inertia force of ± 0.35 of gravity (Sato Kogyo Co. Ltd. 1997).

The restored central columns were built laterally by joining three reinforced concrete-filled tubes (CFTs) with a square cross section of 450×450 mm and a thickness of 12 mm. To evaluate the seismic safety of the new columns, static alternative lateral cyclic loading tests that combine the axial load, including the existing column, were conducted. These experiments confirmed that the load-carrying capacity and performance of the deformation of one cross section of the CFT column are more than 1.5 times that of the existing column and 10 times the design value of the relative displacement, respectively. The new station structure was reconstructed on the original base slab and the bottom of the sidewalls, which were not severely damaged.

Outline of the Numerical Simulation

Numerical Model

In this paper, a numerical simulation of the Daikai Station subway structure influenced by a single upward displacement wave of short duration was performed with a focus on the main section of the station, which suffered severe damage during the Hyogoken-Nanbu earthquake. Fig. 4 shows the numerical analysis model, and Fig. 4(a) shows the discretization of the symmetrical cross section of the whole structure, including the surrounding soils. The soil layers were discretized in the region from the base stratum to the ground surface and laterally more than twice the width of the main section of the station on both sides. The surrounding soils consist of seven layers, among which diluvial deposits (Pleistocene clay, sand, and gravel) have been overlain by alluvial deposits (Holocene clay and sand) (Iida et al. 1996). The decomposed granite soil was used as backfill material for the sidewalls.

The artificial finite boundaries that were previously defined must be set up for the stress waves to ensure that they are not reflected similarly to the infinite domain. In LS-DYNA (Livermore Software Technology Corporation 2016), due to the application of the normal and shear stress waves in Eqs. (1) and (2) to the boundaries, the nonreflecting boundaries for the stress waves were accomplished

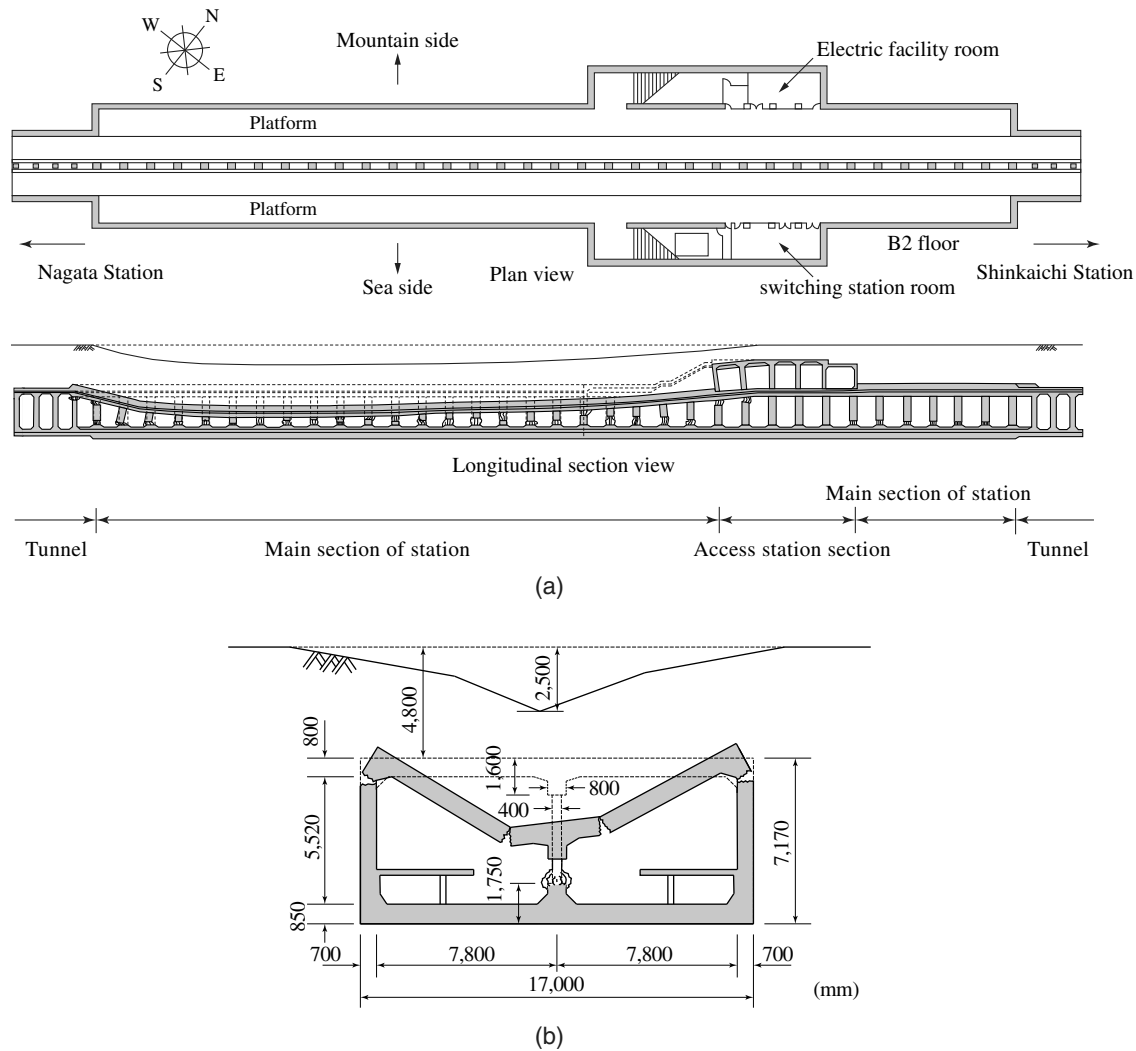


Fig. 3. Damage patterns in the Daikai Station subway structure: (a) longitudinal damage pattern; and (b) damage to the main section.

$$\sigma_{\text{normal}} = -\rho C_d V_{\text{normal}} \dots \quad (1)$$

$$\sigma_{\text{shear}} = -\rho C_s V_{\text{tan}} \dots \quad (2)$$

where ρ , C_d , and C_s = material density, dilatational wave speed, and shear wave speed, respectively, of the transmitting soil layer; the magnitude of these stresses is proportional to the particle velocity of the normal, V_{normal} , and tangential, V_{tan} , respectively.

A contact algorithm with the ability to consider sliding without friction and separating actions was employed for the contacted surfaces of the surrounding soil to all of the outer surfaces of the station structure. Fig. 4(b) shows the 3D discretization of the main section of the station without platforms for the numerical simulation. Because the central columns in the station were arranged at a center-to-center spacing of 3.5 m, a part of the station supported by one column was taken into consideration in the longitudinal direction. Therefore, the length of the station model in the longitudinal direction was 1.75 m considering symmetry. To accurately investigate the dynamic nonlinear behavior of the central column, the concrete for the column and the corresponding upper and lower girders was discretized using cubic elements of approximately 25 mm in length. The rebar pieces were separately discretized by using beam elements, which were perfectly bonded with the concrete elements based on the actual structure of the station before collapse. The rebar and concrete elements were bonded by coupling.

Regarding the boundary conditions, the nodal points on the symmetrical surface and end surface in the longitudinal direction were restrained in the normal directions. The damping factor was ignored because the maximum duration of the forced displacement was only 50 ms and the transient dynamic response characteristics of the station developed during the stress phase due to the propagation of reflection waves. Self-weight was also considered in the numerical analyses.

The applicability of calculation method employed in this study to the transient response analysis of the soil–structure system, which was subjected to a sudden uplift loading, was confirmed by conducting a preliminary elastic analysis and by checking the propagation state of the stress waves and dynamic behavior of the displacement and stress at the free surface and/or nonreflecting boundary of the soil layers. Regarding the failure behaviors of concrete members, by conducting drop-weight impact loading tests of RC beams and numerical simulation of these tests with LS-DYNA, a comparison between the experimental results and numerical results confirmed that the time history of the displacement and crack patterns of the RC beams can be adequately simulated by setting the longitudinal element size of concrete to a length range of 25–35 mm (Kishi et al. 2009, 2011; Kishi and Bhatti 2010). Therefore, the dynamic behavior of the central column may be accurately analyzed in this study.

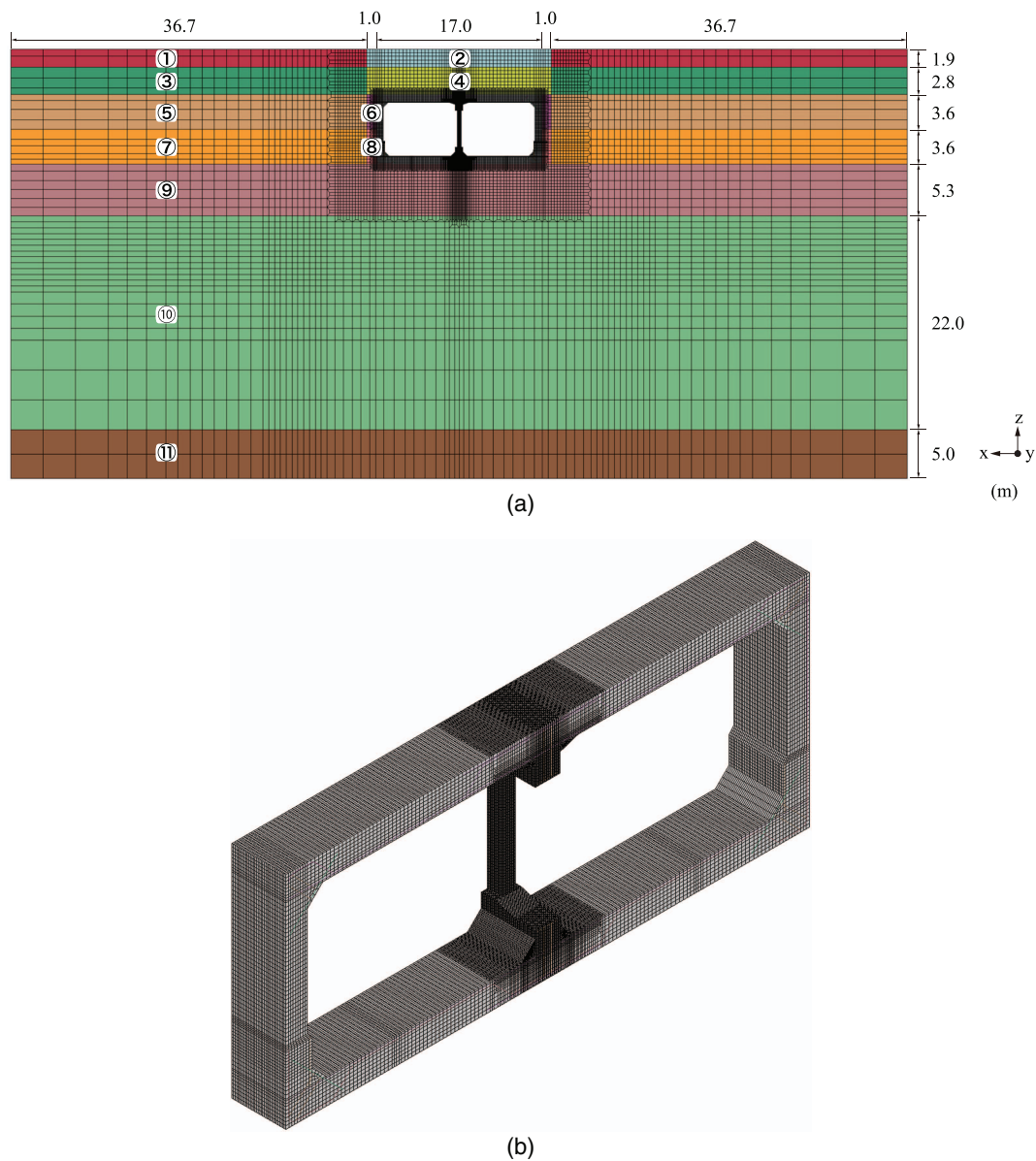


Fig. 4. (Color) Finite-element model of the Daikai Station subway structure: (a) discretization of the cross section including the surrounding soils; and (b) 3D discretization of the main section of the station.

Constitutive Model

Fig. 5 shows the stress-strain relationship for each material used in this numerical analysis: concrete, steel rebar, and overburden and backfilled soils. However, the surrounding soil layers, excluding the remolded soils described previously, were assumed to be elastic. The shear deformation in these layers may be very small due to the lack of lateral loading. The material properties were based on geological survey results obtained by boring and borehole observations, as listed in Table 1 (Iida et al. 1996; Sato Kogyo Co. Ltd. 1997). In this table, the layer numbers refer to those in Fig. 4(a).

A variety of constitutive models for concrete are provided in LS-DYNA (Livermore Software Technology Corporation 2016). In this study, the Karagozian and Case concrete model (KCC model or MAT072R3 in LS-DYNA), as shown in Fig. 5(a), was employed (Malvar et al. 1997) to better regenerate the axial compression failure of concrete. This model can effectively capture key concrete behaviors, including postpeak softening and confinement effects (Wu et al. 2012). Additionally, the model can automatically

generate parameters by inputting the compressive strength f'_c , Poisson's ratio ν_c , density of concrete ρ_c , and the element size (Malvar et al. 2000). These parameters are applied to determine the relationship between the pressure and the volumetric strain. Three kinds of shear strength surfaces, which are yield, maximum, and residual strength surfaces, are utilized to evaluate the damage level, which will be subsequently described. The compressive strength of the concrete was set to $f'_c = 37$ MPa based on Schmidt hammer tests conducted after the earthquake (Sato Kogyo Co. Ltd. 1997). Poisson's ratio and the density were assumed to be $\nu_c = 1/6$ and $\rho_c = 2.3 \times 10^3$ kg/m³, respectively.

By inputting these values and discretizing the concrete into cubic elements with a length of approximately 25 mm, the tensile strength was estimated; the value was approximately 1/10 of the compressive strength, and the compressive stress and tensile stress were released at levels of approximately -0.9% strain and 0.2% strain, respectively. The elastic wave speed of concrete was estimated as $C_c = 3,458$ m/s. The strain-rate effects for the concrete

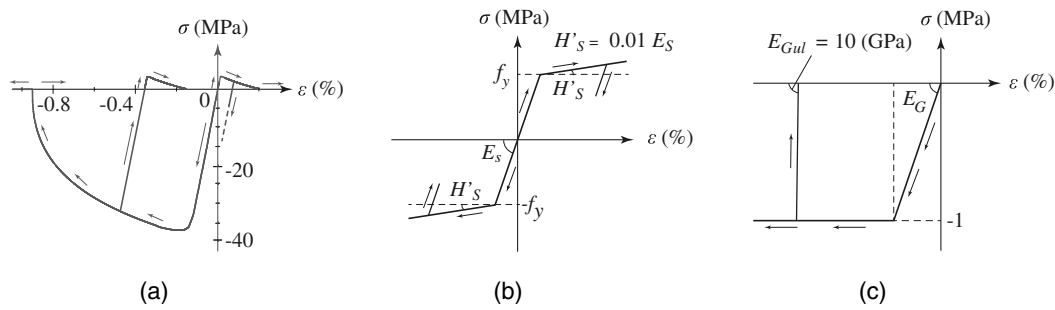


Fig. 5. Constitutive models for materials: (a) concrete; (b) rebar; and (c) overburden soil and backfilled soil.

Table 1. Material properties of soil layers

Layer No.	Soil type	Density, ρ_G (kg/m ³)	Young's modulus, E_G (MPa)	Shear velocity, C_G (m/s)	Compressive strength (MPa)	Yield strain	Poisson's ratio
1	Alluvium clay	1.9×10^3	99	140	1	0.01	0.33
2	Backfill	1.9×10^3	54	100	1	0.018	0.43
3	Alluvium sand	1.9×10^3	111	140	1	0.009	0.49
4	Backfill	1.9×10^3	96	130	1	0.01	0.49
5	Diluvium sand	1.9×10^3	164	170	—	—	0.49
6	Backfill	1.9×10^3	145	160	1	0.007	0.49
7	Diluvium clay	1.9×10^3	205	190	—	—	0.49
8	Backfill	1.9×10^3	146	160	1	0.007	0.49
9	Diluvium clay	1.9×10^3	326	240	—	—	0.49
10	Diluvium gravel	2×10^3	648	330	—	—	0.49
11	Diluvium clay	2.1×10^3	1,544	500	—	—	0.49

were ignored because the numerical analyses conducted in this study concentrated on investigating the qualitative dynamic response characteristics of the structure for upward loading.

Fig. 5(b) shows the stress-strain relationship for the axial and shear rebar used in this study. A bilinear type of constitutive model was applied considering the plastic hardening effect after yielding. The yield strength of the rebar was set to $f_y = 306$ MPa. The density ρ_s , elastic modulus E_s , and Poisson's ratio ν_s for the rebar were assumed using the nominal values of $\rho_s = 7.85 \times 10^3$ kg/m³, $E_s = 206$ GPa, and $\nu_s = 0.3$, respectively. It was assumed that the yielding of the rebar was controlled by the von Mises yield criterion, and the plastic hardening coefficient H'_s was assumed to be 1% of the Young's modulus E_s .

Fig. 5(c) shows the stress-strain relationship for the overburden soils at the station established with a cut-and-cover method and for backfill on the outer side of the walls. The model was assumed to be a perfect elastoplastic body, and the elastic modulus at unloading was $E_{Gul} = 10$ GPa; at this value, the stress was perfectly released as soon as the soil unloaded, and no resistance of the tensile force occurred. The movement of the overburden soils should follow the movement of the ceiling slab when the slab drops due to the collapse of the central column.

Model of Input Uplift Displacement Wave

Assuming a state with a single pulselike uplift motion and a period T_0 at the base stratum, the bottom surface of the stratum was forcibly and linearly moved up to the maximum displacement $d_{i,max}$ during the half time of period T_0 and was then kept at this displacement location. Fig. 6 shows the schematic displacement d_i -time t and velocity V_i -time t relationships. From this figure, the velocity V_i of the movement is obtained as $V_i = 2d_{i,max}/T_0$, and after passing the time of $T_0/2$, the velocity V_i drops to zero. Generally, at the

beginning of loading, when the end of an elastic body vertically impacts a rigid body with velocity V , a wave propagates in the elastic body with an axial stress that is given by the following equation:

$$\sigma = \rho CV \dots \quad (3)$$

where C = elastic wave speed of the body.

Results and Discussion

In this study, a numerical simulation was performed by increasing the velocity of the input displacement (referred to hereinafter as the input velocity) from $V_i = 0.5$ to 4 m/s for two durations of loading: $T_0/2 = 5$ and 50 ms, as mentioned previously, with the former associated with high-frequency ground motion (100 Hz) excited prior to a lateral earthquake input and the latter associated with comparatively low-frequency motion (10 Hz). The maximum displacement $d_{i,max}$ for each velocity V_i is listed in Table 2.

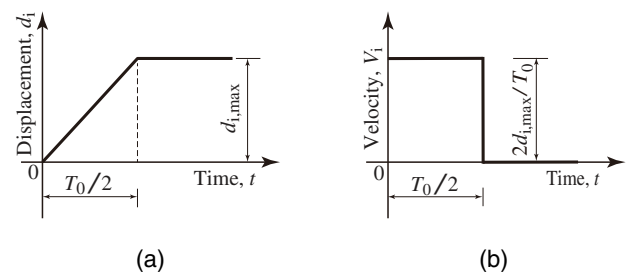


Fig. 6. Schematic time histories of the input wave: (a) displacement d_i ; and (b) velocity V_i .

Time History of Displacement

Figs. 7 and 8 show comparisons of the time histories of the response displacement d and relative displacement d_r at each point.

Table 2. Maximum input displacements

Input velocity, V_i (m/s)	Maximum input displacement, $d_{i,max}$ (mm)	
	Loading duration $T_0/2 = 5$ ms	Loading duration $T_0/2 = 50$ ms
0.5	2.5	25
1	5	50
2	10	100
3	15	150
4	20	200

Figs. 7(a and b) and 8(a and b) are the results for the loading durations of $T_0/2 = 5$ ms and $T_0/2 = 50$ ms, respectively. In these figures, to investigate the propagation characteristics of a wave passing through the station structure from the base stratum, each time history is indicated for points along the axes of the central column and sidewall. Reference time histories for a wave that is not influenced by the substructure are also indicated along the vertical line 10 m inside the free ends of the soil layers.

From the distribution of the reference time histories of the displacement for the soil layers shown in Fig. 7(a), it can be observed that the amplitude of the wave crest gradually decreases up to a similar depth level as that of the lower surface of the base slab and increases near the subsurface layer. The amplitude at the ground surface is almost twice that of the input displacement. This result may be due to the effect of the reflection wave when the axial stress is released at the ground surface.

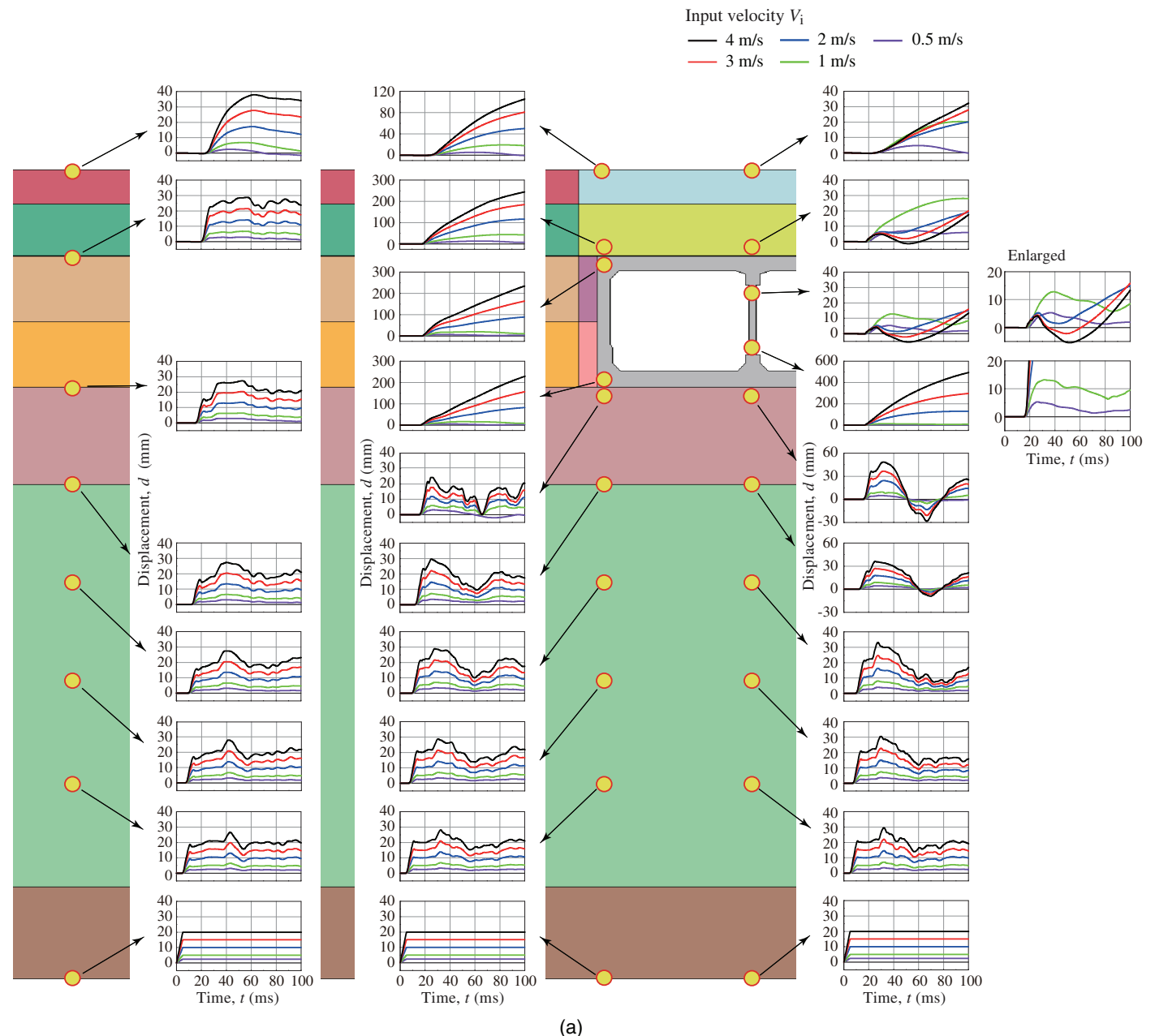


Fig. 7. (Color) Time histories of displacement d : (a) loading duration $T_0/2 = 5$ ms; and (b) $T_0/2 = 50$ ms.

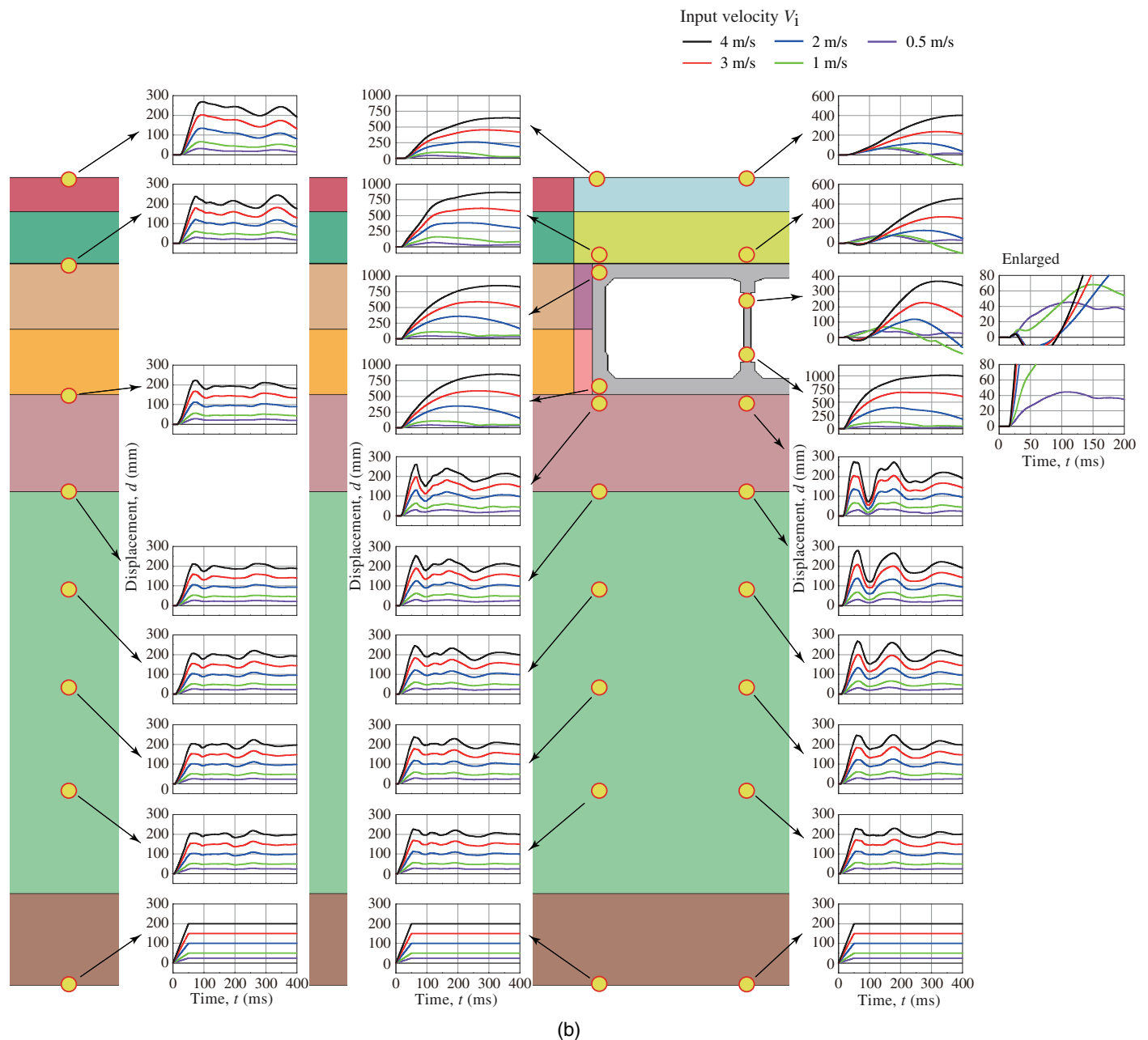


Fig. 7. (Color) (Continued.)

By comparing the time histories of the waves between the lower point of the central column/sidewall and the upper surface point of the soil layer just below the base slab shown in Fig. 7(a), the waves at the column/sidewall monotonically increase, even though the waves behave similarly to $t = 20$ ms after the start of uplift loading (referred to as time t). However, the waves at the soil layer do not increase in amplitude in a similar manner; additionally, the soil layers vibrate alternatively with a period of approximately 60 ms.

Based on the time histories at two column points, when the input velocity is equal to or less than $V_i = 1$ m/s, the wave may propagate continuously. However, by increasing the input velocity V_i by 2 m/s, the displacement at the lower point of the column increases up to approximately $d = 130$ mm, but at the upper point, this value is less than $d = 20$ mm. From Fig. 8(a), these findings are clearly observed from the relative displacement d_r , which

refers to that at the upper point of the soil layer just below the base slab. Thus, the column collapses under axial compression failure because the average axial compressive strain of the column reaches more than $\varepsilon = 2.8\%$ at a 3.82-m column height. By increasing the input velocity to more than $V_i = 2$ m/s, because the amplitude of the wave at the lower point of the column increases more than that at $V_i = 2$ m/s, the column will suffer severe damage. Because the time histories of the waves between two points on the sidewall are approximately the same, the average axial strain in the wall may be very small, and the wall may not reach axial compressive failure, thus differing from the column state. This discrepancy may be inferred from the difference in axial stiffness between the column and wall.

From Fig. 8(a), because the relative displacement d_r at the ground surface on the axis of the sidewall, which refers to that of the ceiling slab, is distributed in the negative region and reaches

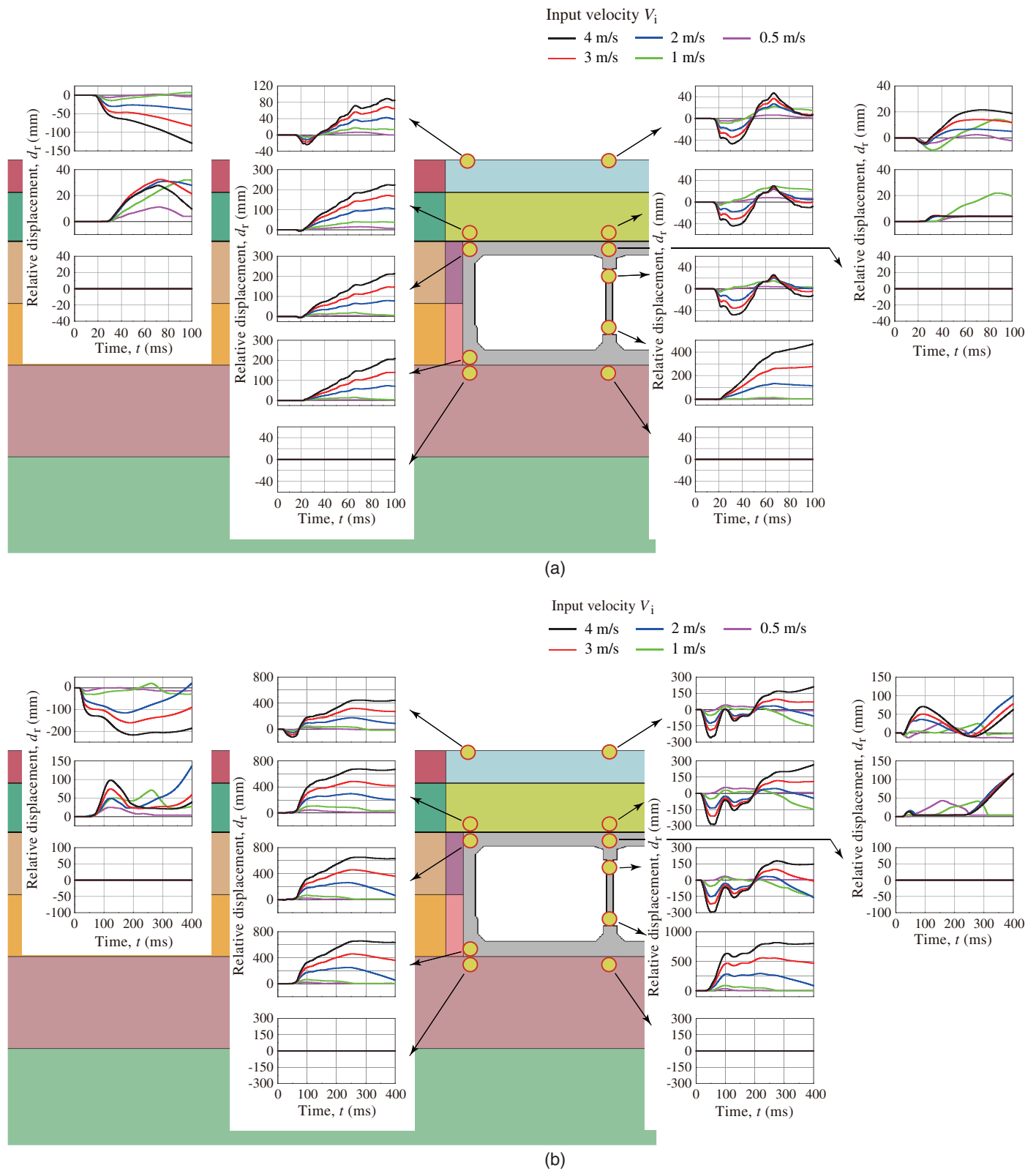


Fig. 8. (Color) Time histories of the relative displacement d_r , which refers to the displacements at the upper point of the soil layer just below the base slab and at the ceiling slab: (a) loading duration $T_0/2 = 5$ ms; and (b) $T_0/2 = 50$ ms.

a maximum of approximately 150 mm, the displacement at the ground surface above the sidewall may be restrained significantly compared with that of the sidewall. Alternatively, the ground surface on the axis of the central column moves slightly upward because the maximum relative displacement $d_{r,max}$ at the ground

surface, which refers to that at the ceiling slab, is approximately 20 mm.

Fig. 7(b) shows the results for the case of a loading duration of $T_0/2 = 50$ ms. The distribution of the reference time histories of the waves for the soil layers show that although the amplitude of the

wave at the ground surface is increased due to the effect of the reflection wave, in each soil layer, this amplitude is similar to that of the input displacement.

The distribution of the time histories of displacement along two axes shows that the wave at the upper surface of the soil layer just below the base slab cannot propagate continuously to the lower points of the central column/sidewall, as in the case of a loading duration of $T_0/2 = 5$ ms. The soil layers separate from the base slab and change to a vibration state with a period of approximately $T = 150$ ms, and the period is prolonged from $T = 60$ to 150 ms due to the loading duration extending from 5 to 50 ms.

The results of the time histories of the displacements at both the upper point and lower point of the central column indicate that when the input velocity is $V_i = 0.5$ m/s, the wave propagates continuously in the upward direction. However, when the input velocity V_i is increased above 0.5 m/s, the amplitude of the wave at the lower point increases abruptly, but at the upper point, the amplitude does not reach half that at the lower point and the relative displacement is distributed almost in the negative region to time $t = 200$ ms, as shown in Fig. 8(b). The strain in the column at time $t = 50$ ms is estimated when the input velocity $V_i = 1$ m/s and the displacement amplitudes at the lower and upper points of the column are approximately $d = 70$ and 10 mm, respectively. Notably, the average axial compressive strain is greater than $\varepsilon = 1.5\%$, and the column may collapse under axial compression failure. Therefore, by increasing the input velocity V_i , the column may experience increasingly severe damage.

Regarding the dynamic response of the sidewall, because the wave continuously propagates in the upward direction along the wall, severe damage does not occur, irrespective of the duration of loading.

From Fig. 8(b), it is observed that the relative displacements d_r at the ground surface on the two axes, which refers to each distribution at the ceiling slab, are approximately 50 mm larger than those in the case of a loading duration of $T_0/2 = 5$ ms [Fig. 8(a)]. However, the distribution characteristics are almost similar to time $t = 100$ ms. When the input velocity is equal to or greater than $V_i = 2$ m/s, because the relative displacement d_r at the bottom of the overburdened soils on the axis of the central column, which refer to that of the ceiling slab, abruptly increases at time approximately $t = 250$ ms, the overburden soils separate from the ceiling slab and begin to substantially rise.

Time History of the Particle Velocity

Fig. 9 shows comparisons of the time histories of the particle velocity V at each point, which are similar to those for the displacement d shown in Fig. 7. Fig. 9(a) indicates the results for a loading duration of $T_0/2 = 5$ ms. The distribution of the reference time histories for the soil layers shows that at the beginning of wave propagation, the amplitude of the wave remains near the input value in each soil layer, except at the base of the second subsurface layer and at the ground surface; the values at these locations are largely influenced by the reflection wave due to the axial stress reaching zero at the ground surface. Then, the positive-sign reflection wave propagates in the downward direction.

From the distribution of the time histories of the wave along the two other axes, because the displacement wave cannot propagate continuously at the boundary between the bottom of the base slab and the upper surface of the soil layer, as mentioned previously, wave discontinuity can be observed. Although the reflection wave with a positive sign propagates in the downward direction in the soil layers, the upper surface of the soil layer below the base slab acts as a free boundary. Because the time histories at the bottom

surface points of the overburden soils and the upper points of the column/sidewall are different, the overburden soils may separate slightly from the ceiling slab at some time.

Based on a comparison of the time histories of the particle velocity V at the two points on the column, when the input velocity is equal to or greater than $V_i = 2$ m/s, the amplitude of the wave at the lower point maintains an approximately similar value after separation from the soil layer and then gradually decreases. Additionally, at the upper point, the amplitude remains less than $V = 1.5$ m/s and decreases to a negative value. This result suggests that due to the comparatively low axial stiffness of the column, the column may reach axial compression failure, and the stress wave at the beginning of loading may not directly propagate toward the upper part of the column. The axial stress in the column due to particle movement was estimated. The maximum particle velocities V_{\max} in the case of the input velocities $V_i = 2, 3,$ and 4 m/s are approximately $V_{\max} = 4.5, 7,$ and 10 m/s, respectively, and the stress that corresponds to each maximum velocity V_{\max} is evaluated, assuming that the concrete column is an elastic body, using Eq. (3) with $\sigma = 36, 56,$ and 60 MPa. From these results, as discussed in the previous section, it is confirmed that the column may collapse with axial compression failure because the compressive strength of the concrete was $f'_c = 37$ MPa.

When the input velocity is $V_i = 1$ m/s, the particle velocity V at the upper point of the column is approximately $V = 1$ m/s at approximately $t = 25$ ms and then decreases approximately linearly to zero at time $t = 40$ ms. Moreover, at the lower point, even though the velocity V at time $t = 20$ ms is greater than $V = 1.5$ m/s, the velocity decreases to zero around $t = 30$ ms. This change suggests that after time $t = 25$ ms, the reflection wave from the upper point may not directly propagate to the lower point, potentially because horizontal circumferential cracks may occur along the column, and the stress wave may disappear, as supported by the axial stress trend at a particle velocity of $V = 0.5$ m/s and tensile stress of $\sigma = 4$ MPa at time $t = 30$ ms.

Fig. 9(b) shows comparisons of the time histories of the particle velocity V for a loading duration of $T_0/2 = 50$ ms. The reference time histories of the wave with depth in the soil layers show that the distribution characteristics of the wave are similar to those for a loading duration of $T_0/2 = 5$ ms. However, the amplitude of each wave during uplift loading abruptly increases, which implies that the reflection wave propagating in the downward direction from the ground surface influences the time history for a long duration of loading. After unloading, the soil layers reach the free vibration state.

From the distributions of the time histories of the wave along the two axes, the response characteristics of the waves are similar to those in the case of a loading duration of $T_0/2 = 5$ ms, except that the amplitude of the wave at each point in the soil layers below the base slab abruptly increases, thus mimicking the reference time histories.

Deformation and Damage Patterns of the Station

In the LS-DYNA code, the KCC model is applied as the constitutive model for concrete, and the damage level of a concrete element can be evaluated using an index (Malvar et al. 1997; Markovich et al. 2011). In the KCC model, three independent strength surfaces are formulated as follows:

$$F_i(p) = a_{0i} + \frac{p}{a_{1i} + a_{2i}p} \quad (4)$$

where $i = y, m,$ and r , i.e., the yield strength surface, maximum strength surface, and residual strength surface, respectively; $p =$ pressure; and a_{ji} ($j = 0, 1, 2$) = parameters calibrated from the test data, which are set as default parameters in LS-DYNA

(Livermore Software Technology Corporation 2016). The failure surface is interpolated between the maximum strength surface and either the yield strength surface or the residual strength surface. The failure surface is a function of the internal damage parameter λ , which is defined

$$\lambda = \int_0^{\bar{\varepsilon}^p} \frac{d\bar{\varepsilon}^p}{[1 + (s/100)(r_f - 1)](1 + (p/r_f f_t))^{b_1}} \quad \text{when } p \geq 0 \quad (5)$$

$$\lambda = \int_0^{\bar{\varepsilon}^p} \frac{d\bar{\varepsilon}^p}{[1 + (s/100)(r_f - 1)](1 + (p/r_f f_t))^{b_2}} \quad \text{when } p < 0 \quad (6)$$

where the effective plastic strain increment $d\varepsilon^p$ is given by

$$d\varepsilon^p = \sqrt{\left(\frac{2}{3} d\varepsilon_{ij}^p d\varepsilon_{ij}^p\right)} \quad (7)$$

where f_t = tensile strength of concrete; b_1 and b_2 = damage scaling parameters for the case of uniaxial compression and tension, respectively; r_f = dynamic increase factor that accounts for the strain rate effects; and s = user-defined scale of the damage measure. These parameters excluding s are set as default parameters in LS-DYNA (Livermore Software Technology Corporation 2016). The parameter s can range from 0 to 100. In the case of $s = 0$, the strain-rate effects are omitted; for $s = 100$, the strain rate effects

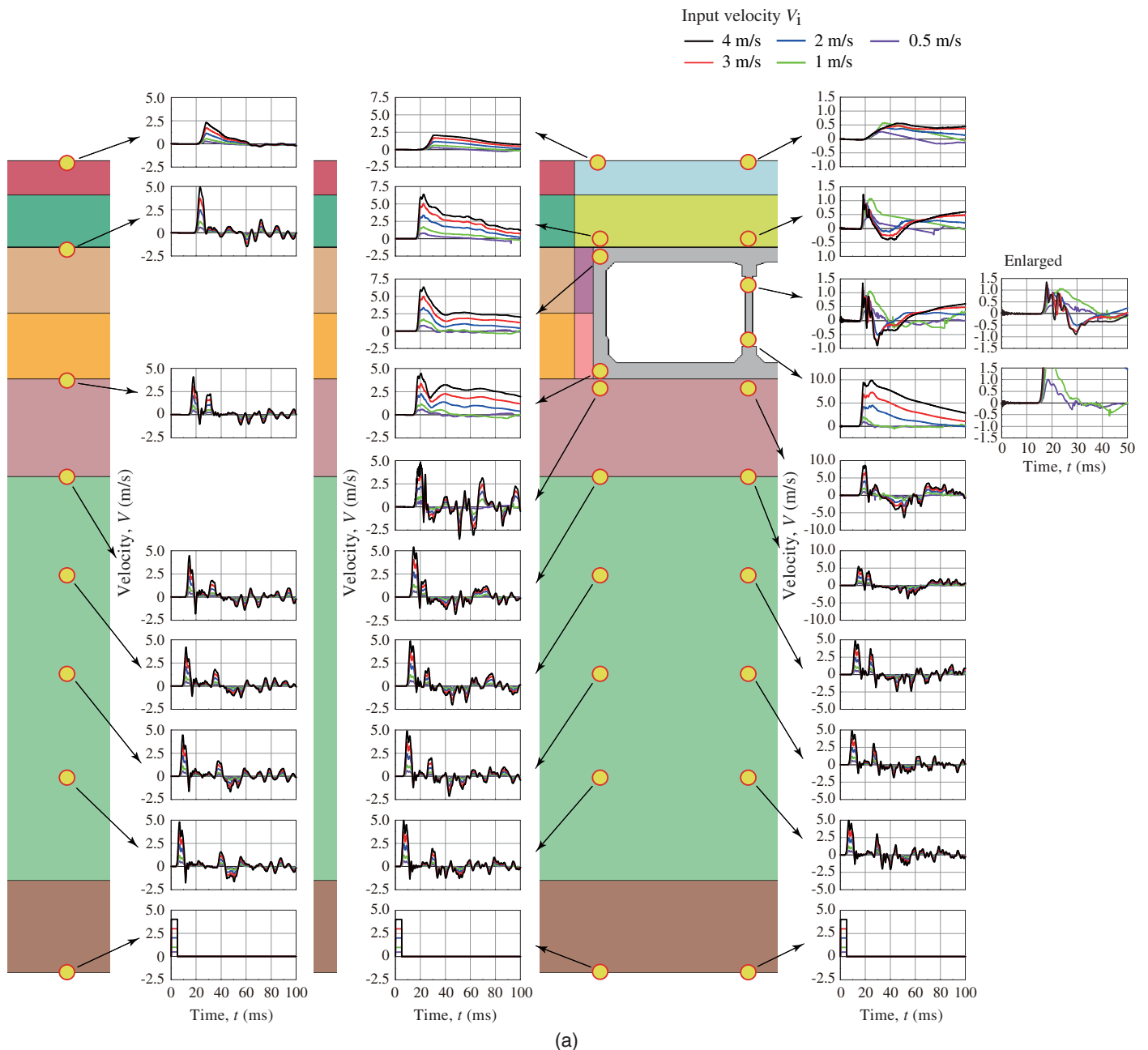


Fig. 9. (Color) Time histories of the particle velocity V : (a) loading duration $T_0/2 = 5$ ms; and (b) $T_0/2 = 50$ ms.

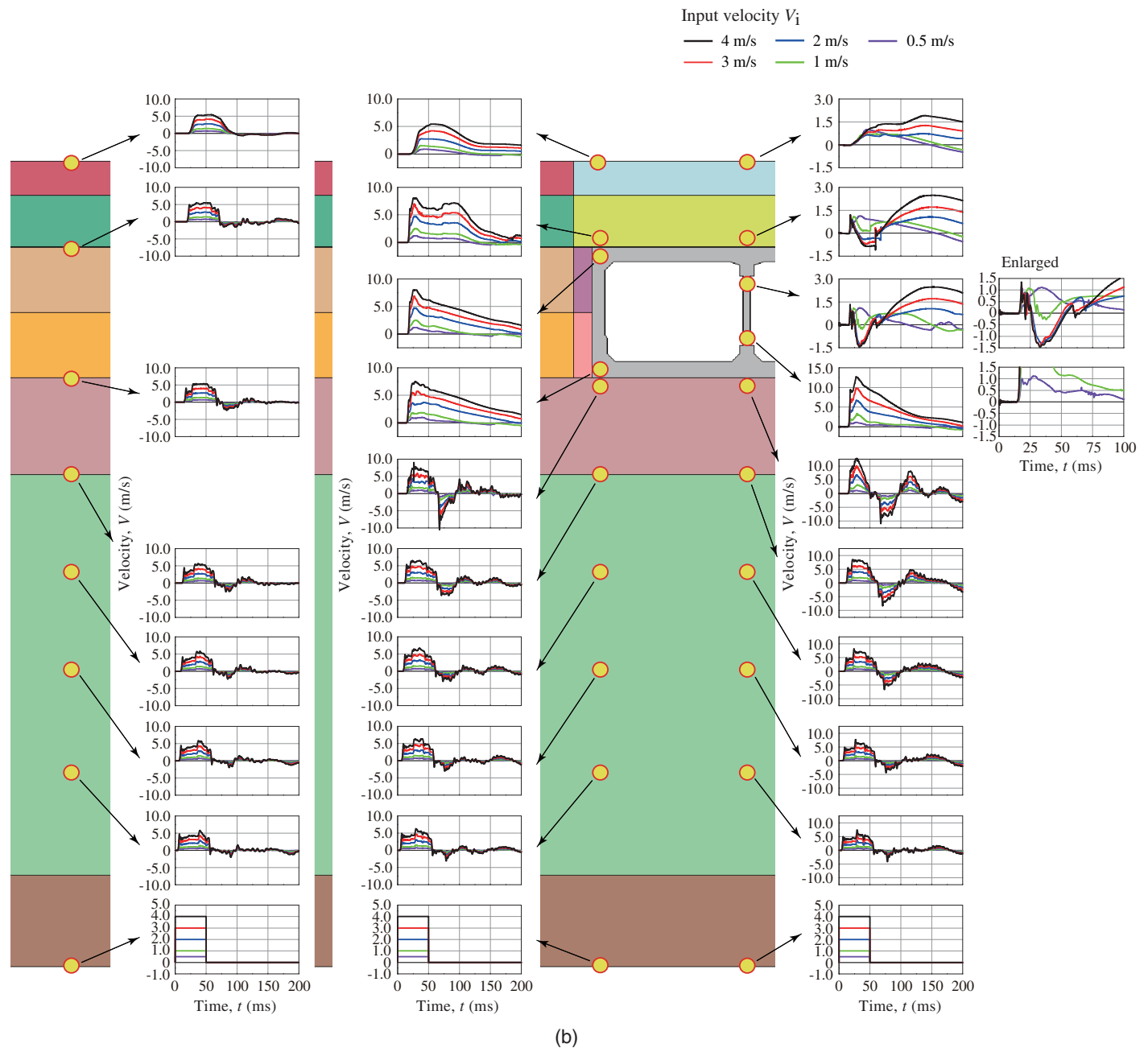


Fig. 9. (Color) (Continued.)

are fully included. In this study, the strain rate effects were omitted, as previously described. When the failure surface is distributed in the region between the yield strength surface and the maximum strength surface and between the maximum strength surface and the residual strength surface, the damage index was defined to move linearly from 0 to 1 and from 1 to 2, respectively. More details have been provided by Malvar et al. (1997) and Markovich et al. (2011).

In this study, it is assumed that the element reaches the ultimate state when the damage index is equal to or greater than 1.98, and elements that reach this value are colored red.

Fig. 10 shows the changes in the deformation and damage patterns in the cross section of the structure for each input velocity V_i at time $t = 100$ and 400 ms and loading duration $T_0/2 = 5$ and 50 ms; additionally, the enlargement factor for the deformation is set to 1.

Fig. 10(a) shows the results in the case of the loading duration $T_0/2 = 5$ ms. From this figure, when the input velocity $V_i = 1$ m/s, horizontal circumferential cracks form over the entire height of the central column, and the ceiling and base slab are subjected to positive and negative bending moments, respectively, based on the flexural crack patterns. Horizontal circumferential cracks may occur due to the downward propagation of the reflection wave, as mentioned in the previous section, and the cracks observed in the RC bridge piers (Fig. 11) after the Hyogoken-Nanbu earthquake may be due to the same phenomenon associated with these crack patterns. At an input velocity of $V_i = 2$ m/s, the central column collapses around midheight, and the base slab tends to move up and separate from the soil layer. Upon increasing the input velocity V_i , the magnitude of the axial compression failure of the column increases, and the area tends to move in the downward direction. As mentioned

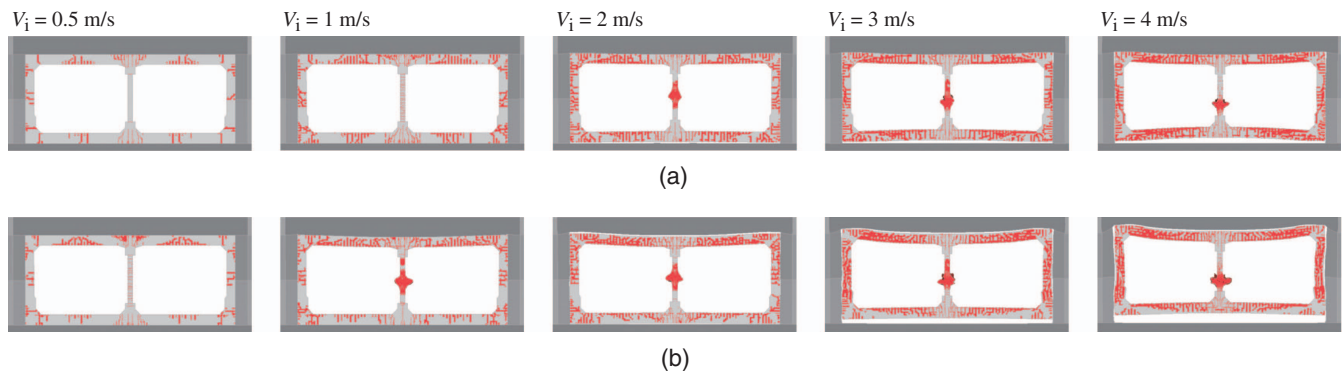


Fig. 10. (Color) Deformation and damage patterns in the station structure: (a) at time $t = 100$ ms for loading duration $T_0/2 = 5$ ms; and (b) at time $t = 400$ ms in case of $T_0/2 = 50$ ms.

previously, the central column partially fails, but the sidewall does not, and only flexural cracks occur.

From Fig. 10(b), for a loading duration of $T_0/2 = 50$ ms, horizontal circumferential cracks occur at an input velocity of $V_i = 0.5$ m/s, even though an indication of this phenomenon is not clearly stated in the previous sections. Additionally, the central column reaches axial compression failure at $V_i = 1$ m/s, and the damage level of the column may increase due to the long duration of loading. Both the base slab and ceiling slab are in a state of separation from the soil layer when the input velocity is greater than $V_i = 1$ m/s.

Temporal Transition of Deformation and Damage Patterns for the Structure and Surrounding Soils

Fig. 12 shows comparisons of the time histories of the displacement at the ground surface point and upper point of the central column, the relative displacement at the bottom of the overburden soils and upper surface of the ceiling slab, and relative displacement at the upper and lower points of the column along the column axis at the input velocity of $V_i = 4$ m/s and loading duration of $T_0/2 = 5$ ms. Notably, the ground surface rises to a height of 90 mm because the base slab is lifted and then gradually falls to more than 600 mm below the original ground level due to the axial compression failure of the column and the effect of the self-weight of the

soils. Additionally, the overburden soils separate from the ceiling slab with a maximum distance of approximately 100 mm and contact the slab again due to the effect of gravity after a time of approximately $t = 500$ ms. Because the relative displacement between the upper point and lower point of the column increases monotonically to more than 500 mm due to uplift loading, the axial compression failure of the column proceeds continuously. Even the relative displacement maintains a constant value when the overburden soils separate from the ceiling slab. After the soils contact the slab again due to gravity, the displacement gradually increases, and the compression failure of the column proceeds.

Fig. 13 shows the temporal transitions of the deformation and damage patterns in the cross section of the station structure and overburdened soils 1,000 ms from the beginning of loading based on the case presented in Fig. 12. This figure confirms that due to uplift loading, the base slab is lifted, the central column reaches axial compression failure, and the overburden soils separate from the ceiling slab at a time of approximately $t = 400$ ms. Due to the effect of gravity, the overburden soils contact the ceiling slab again, the cross section of the structure gradually falls with the overburden soils, and the compression failure of the column proceeds.

As shown in Fig. 3(b), the damage state of the Daikai Station subway structure reached during Hyogoken-Nanbu earthquake is described as follows: (1) the central columns were shortened due to axial compression failure; (2) the upper areas of the sidewalls and ceiling slab near the central column perfectly broke in flexure and folded out sharply and symmetrically; and (3) a maximum subsidence of the ground surface above the central column reached 2.5 m. The numerical results indicate that even though the sidewalls and ceiling slab were damaged significantly and



Fig. 11. (Color) Example of horizontal circumferential cracks that occurred in an RC bridge pier. (Image by Keiichiro Sonoda.)

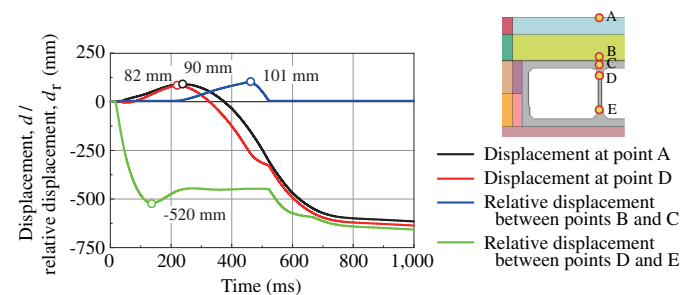


Fig. 12. (Color) Comparisons of the time histories of displacement and relative displacement on the axis of the central column for an input velocity $V_i = 4$ m/s and loading duration $T_0/2 = 5$ ms.

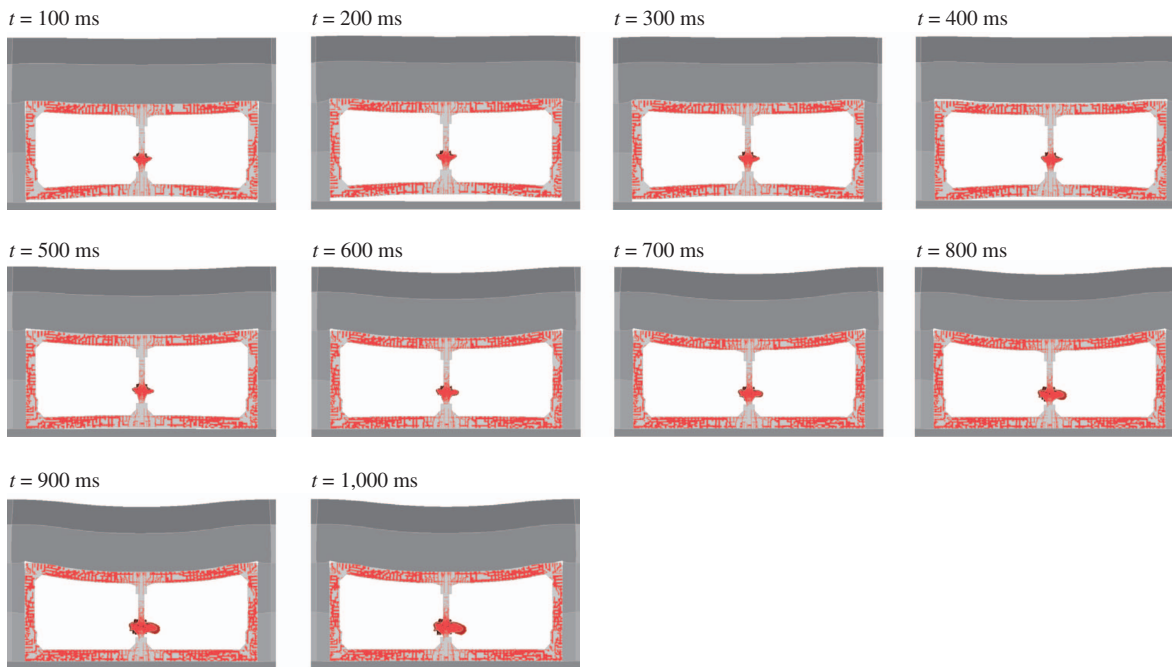


Fig. 13. (Color) Temporal transitions of deformation and damage patterns in the station structure and overburden soils for an input velocity $V_i = 4$ m/s and loading duration $T_0/2 = 5$ ms.

deformed symmetrically, they have not perfectly broken in flexure and the maximum subsidence of the ground surface did not reach 2.5 m but reached approximately 0.6 m. However, because the failure characteristics of the station structure obtained from this study are approximately similar to those of the actual structure during the Hyogoken-Nanbu earthquake, the magnitude of the actual damage level may be reproduced due to the increase in the input velocity and/or the duration of displacement loading. Thus, the potential for collapse of the central column of the Daikai Station subway structure due to impulse uplift loading may be confirmed.

Conclusions

In this study, to investigate the dynamic behavior of the Daikai Station subway structure due to impulse upward loading, a 3D elastoplastic transient response analysis was performed considering the surrounding soils, the isolated pulselike upward displacement from the bedrock, and varying input velocities and loading durations. The results obtained in this study were as follows:

- During displacement and wave propagation in the upward direction, the wave amplitudes increase significantly at the lower point of the central column, the column reaches a state of axial compression failure, and the base slab separates from the soil layer.
- Although the amplitude of the waves generally increased at the lower point of the sidewall, the waves continued to propagate in the upward direction, and the wall did not experience severe damage because it had a large axial stiffness compared with that of the column.
- These aforementioned characteristics were observed for not only long durations of loading, such as 50 ms but also for short durations, such as 5 ms. Additionally, damage increased with increasing input velocity.
- When the input velocity is small, axial compression failure in the column is not reached, but horizontal circumferential cracks

occur in the column due to the effect of the tensile reflection wave.

- The Daikai Station subway structure may have collapsed due to impulse upward loading because the central column was shortened as a result of axial compression failure and the ground surface significantly settled due to the effects of gravity and earthquake actions. This result was confirmed by numerical analysis.

Parameter study of the dynamic behavior of the station structure, in which the surrounding soil distribution and/or constitutive models of the materials are varied, may be a future issue.

Data Availability Statement

All data generated or used during the study appear in the published article.

Acknowledgments

A photo used in Fig. 2 was reprinted through the courtesy of Dr. S. Sakurai, Professor Emeritus of Kobe University, Japan, and the Japanese Society of Rock Mechanics (JSRM). The authors would like to thank Professor Sakurai and JSRM for their cooperation.

References

- An, X., A. A. Shawky, and K. Maekawa. 1997. "The collapsed mechanism of a subway station during the Great Hanshin earthquake." *Cem. Concr. Compos.* 19 (3): 241–257. [https://doi.org/10.1016/S0958-9465\(97\)00014-0](https://doi.org/10.1016/S0958-9465(97)00014-0).
- EERC (Earthquake Engineering Research Center). 1995. *Geotechnical reconnaissance of the effects of the January 17, 1995, Hyogoken-Nanbu earthquake, Japan*. UCB EERC-95/01. Berkeley, CA: Univ. of California at Berkeley.

- Hanshin Expressway Public Corporation. 1995. *Report on damage to the Hanshin Expressway during the Hyogoken-Nanbu earthquake*. [In Japanese.] Osaka, Japan: Hanshin Expressway Public Corporation.
- Huo, H., A. Bobet, G. Fernandez, and J. Ramirez. 2005. "Load transfer mechanisms between underground structure and surrounding ground: Evaluation of the failure of the Daikai station." *J. Geotech. Geoenviron. Eng.* 131 (12): 1522–1533. [https://doi.org/10.1061/\(ASCE\)1090-0241\(2005\)131:12\(1522\)](https://doi.org/10.1061/(ASCE)1090-0241(2005)131:12(1522)).
- Iida, H., T. Hirota, N. Yoshida, and M. Iwafuji. 1996. "Damage to Daikai subway station." *Soils Found.* 36: 283–300. https://doi.org/10.3208/sandf.36.Special_283.
- Japan Road Association. 1996. *Design specification of highway bridges, Part V: Seismic design*. Tokyo: Chiyoda.
- Kawashima, K., and S. Unjoh. 1997. "Impact of Hanshin/Awaji earthquake on seismic design and seismic strengthening of highway bridges." *J. Jpn. Soc. Civ. Eng.* 556 (Jan): 1–30.
- Kishi, N., and A. Q. Bhatti. 2010. "An equivalent fracture energy concept for nonlinear dynamic response analysis of prototype RC girders subjected to falling-weight impact loading." *Int. J. Impact Eng.* 37 (1): 103–113. <https://doi.org/10.1016/j.ijimpeng.2009.07.007>.
- Kishi, N., S. G. Khasraghy, and H. Kon-No. 2011. "Numerical simulation of reinforced concrete beams under consecutive impact loading." *ACI Struct. J.* 108 (4): 444–452. <https://doi.org/10.14359/51682984>.
- Kishi, N., S. Okada, and H. Kon-No. 2009. "Numerical impact response analysis of rockfall protection galleries." *Struct. Eng. Int.* 19 (3): 313–320. <https://doi.org/10.2749/101686609788957766>.
- Livermore Software Technology Corporation. 2016. *LS-DYNA user's manual version R9*. Livermore, CA: Livermore Software Technology Corporation.
- Li, W., and Q. Chen. 2018. "Seismic performance and failure mechanism of a subway station based on nonlinear finite element analysis." *KSCCE J. Civ. Eng.* 22 (2): 765–776. <https://doi.org/10.1007/s12205-017-1840-y>.
- Maekawa, K., A. Pimanmas, and H. Okamura. 2003. *Nonlinear mechanics of reinforced concrete*. London: Spon.
- Malvar, L. J., J. E. Crawford, and K. B. Morill. 2000. *K&C concrete material model release III: Automated generation of material model input*. TR-99-24.3. Glendale, CA: Karagozian & Case.
- Malvar, L. J., J. E. Crawford, J. W. Wesevich, and D. Simons. 1997. "A plasticity concrete material model for DYNA3D." *Int. J. Impact Eng.* 19 (9–10): 847–873. [https://doi.org/10.1016/S0734-743X\(97\)00023-7](https://doi.org/10.1016/S0734-743X(97)00023-7).
- Markovich, N., E. Kochavi, and G. Ben-Dor. 2011. "An improved calibration of the concrete damage model." *Finite Elem. Anal. Des.* 47 (11): 1280–1290. <https://doi.org/10.1016/j.finel.2011.05.008>.
- Matsuda, T., H. Ouchi, and S. Samata. 1997. "Seismic damage analysis on box culvert with intermediate columns." [In Japanese.] *J. Jpn. Soc. Civ. Eng.* 563/I-39 (Apr): 125–136.
- Parra-Montesinos, G. J., A. Bobert, and J. Ramirez. 2006. "Evaluation of soil-structure interaction and structural collapse in Daikai subway station during Kobe earthquake." *ACI Struct. J.* 103 (1): 113–122. <https://doi.org/10.14359/15092>.
- Sakurai, S. 2014. "Case studies on the dynamic behavior of tunnels caused by Hyogoken-Nanbu earthquake whose epicenter was very close to the tunnels." In *Proc., ISRM Int. Symp.—8th Asian Rock Mechanics Symp.*, Salzburg, Austria: International Society for Rock Mechanics and Rock Engineering.
- Sato Kogyo. 1997. *Document on disaster recovery of the Daikai station for the Tozai line of the Kobe rapid transit system*. [In Japanese.] Tokyo: Sato Kogyo.
- Sonoda, K., and H. Kobayashi. 1996. "On the impact-like failure of reinforced concrete structures by Hyogo-ken Nanbu earthquake (Kobe, 1995)." In *Proc., 1st Int. Conf. on Earthquake Resistant Engineering Structures*, 693–704. Southampton, UK: Computational Mechanics Publications.
- Sonoda, K., H. Kobayashi, and K. Nagano. 1997a. *On evidences of strong vertical ground motions at an early stage of the Hyogo-ken Nanbu earthquake*. [In Japanese.] Osaka, Japan: Osaka City Univ.
- Sonoda, K., H. Kobayashi, and T. Nakajima. 1997b. *A consideration of impact-like failure of RC columns in a subway station*. [In Japanese.] Osaka, Japan: Osaka City Univ.
- Uenishi, K., and S. Sakurai. 2000. "Characteristic of the vertical seismic waves associated with the 1995 Hyogo-ken Nanbu (Kobe), Japan earthquake estimated from the failure of the Daikai underground station." *Earthquake Eng. Struct. Dyn.* 29 (6): 813–821. [https://doi.org/10.1002/\(SICI\)1096-9845\(200006\)29:6<813::AID-EQE939>3.0.CO;2-E](https://doi.org/10.1002/(SICI)1096-9845(200006)29:6<813::AID-EQE939>3.0.CO;2-E).
- Uenishi, K., and S. Sakurai. 2014. "The generation of seaquakes and its impact on floating bodies." *Int. J. Protective Struct.* 5 (2): 207–218. <https://doi.org/10.1260/2041-4196.5.2.207>.
- Wu, Y., J. E. Crawford, and J. M. Magallanes. 2012. "Performance of LS-DYNA concrete constitutive models." In *Proc., 12th Int. LS-DYNA Users Conf.* Livermore, CA: Livermore Software Technology Corporation.
- Yu, H., and X. Li. 2017. "Investigation on damage mechanism of the Daikai station induced by the strong Kobe earthquake." *Int. J. Earth Environ. Sci.* 2 (147): 10. <https://doi.org/10.15344/2456-351X/2017/147>.